Contents list available at CBIORE journal website

International Journal of Renewable Energy Development

Journal homepage: https://ijred.cbiore.id

Research Article

Chemically activated biochar derived from mangrove litter with enhanced CO_2 adsorption capacity for carbon sequestration

Dessy Ariyanti[a,b*], Viona Syifa[a,b], Farida Diyah Hapsari[b,c], I Nyoman Widiasa[a], Widayat Widayat[a], Silviana Silviana[a], Aprilina Purbasari[a], Herma Dina Setiabudi[d], Fazlena Hamzah[e]

[a]*Department of Chemical Engineering, Faculty of Engineering, Universitas Diponegoro, Tembalang, Semarang, Indonesia*

[b]*Center of Advanced Material for Sustainability, Universitas Diponegoro, Tembalang, Semarang, Indonesia*

[c]*Department of Chemical Engineering, Universitas Pattimura, Ambon 97134, Indonesia*

[d]*Faculty of Chemical & Process Engineering Technology, Universiti Malaysia Pahang Al-Sultan Abdullah, Pahang, Malaysia*

[e] *School of Chemical Engineering, Universiti Teknologi MARA (UiTM), Malaysia*

Abstract. Overcoming climate change is crucial to ensure environmental sustainability. This research focuses on the development of chemically activated biochar (CAB) from mangrove litters that can be used for CO_2 adsorption, which leads to reducing the impacts of climate change. The synthesisation of CAB was carried out via pyrolysis at 400°C for 2 hours under nitrogen gas flow, followed by treatment using various activating agents (0.1 M of H_2SO_4, HCl, KOH, and NaOH) for 2 hours with a biochar-to-solution ratio of 1 g : 4 mL. The activation process was designed to enhance surface area, pore characteristics, and functional groups associated with CO_2 adsorption performance. The observation on the characteristics of CAB using Scanning Electron Microscope and Energy Dispersive X-Ray (SEM-EDX), The Brunauer, Emmett, Teller and Barret-Joyner-Halenda (BET-BJH), Fourier Transform Infrared Spectroscopy (FTIR), CHN Analyser, and static batch CO_2 adsorption tests shows the ability of CAB in capturing CO_2 through several possible mechanism. Among the samples, KOH-activated biochar (B-KOH) exhibited the highest CO_2 adsorption capacity, reaching 12.47 mmol CO_2 g^{-1} biochar. This high performance is attributed to a potassium (K) composition of 9.74%, which effectively catalyzed the development of a microporous structure, resulting in a micropore volume of 5.927 x 10^{-3} cm^3/g and an optimized average pore width of 1.543 nm. Furthermore, B-KOH maintained the highest O-H group area (1.533 a.u. x cm^{-1}), enhancing its affinity for CO_2 molecules. This research offers an innovative and practical solution to reduce greenhouse gases and is expected to have a significant impact, both locally and globally, in advancing sustainable development.

Keywords: adsorption, biochar, carbon sequestration, chemical activation, mangrove litters

Received: 5th Dec 2025; Revised: 19th January 2026; Accepted: 8th February 2026; Available online: 22nd February 2026

1. Introduction

Climate change and global warming are global phenomena that cause melting of polar ice, ecosystem disruption, sea level rise, and extreme weather events such as storms, strong winds, and floods (Promakhova *et al.,* 2019). The primary driver of climate change is CO_2 emissions, which have increased from 280 ppm to 416 ppm by volume, reaching approximately 1 gigaton in the atmosphere over the last 3 to 10 centuries (Pradhan *et al.,* 2024). To limit the global temperature rise below 2°C, 125 countries signed the 2015 Paris Agreement, requiring substantial CO_2 emission reductions through a comprehensive decarbonization strategy, including Carbon Capture and Storage (CCS) technology (Agency EP, 2022; Wolicki *et al*., 2024). Research on CO_2 capture by olive pomace biochar indicates that it can adsorb 0.402 mmol CO_2/g biochar (Sundaramoorthy *et al.,* 2023; Monteagudo et al., 2026).

Biochar is a carbon-rich material produced from biomass through pyrolysis under oxygen-limited conditions (Amalina *et al.,* 2022; Ong *et al* 2024). Various biomass sources, including rice husks, bagasse, and mangrove litter, can be used to produce biochar, supporting sustainable biomass utilization and reducing greenhouse gas emissions from natural decomposition (Wijitkosum, 2022). Biochar has potential as a CO_2 adsorbent, which is governed by pore structure, functional groups, and surface area (Guarin et al., 2025). However, biochar produced via direct pyrolysis generally shows limited adsorption capacity (Deng *et al.,* 2024). Therefore, surface modifications are necessary to enhance adsorption.

The CO_2 adsorption of biochar can be enhanced through physical, chemical, or physicochemical modifications. Chemical activation increases surface area, porosity, and surface charge, thereby improving adsorption capacity (Zhi *et al.,* 2025). Chemical activation of woodchip biochar using KOH has been reported to achieve 5.29 mmol CO_2 /g biochar (Faggiano *et al.,* 2025). In addition, pine-based biochar activated using pure CO_2 showed an adsorption capacity of 2.1 mmol CO_2 /g biochar (Abbaspour *et al.*, 2025). Recent studies indicate that CO_2 adsorption in biochar is increasingly governed by pore structure

* Corresponding author
Email: dessy.ariyanti@che.undip.ac.id (D. Ariyanti)

https://doi.org/10.61435/ijred.2026.62059
ISSN: 2252-4940/© 2026.The Author(s). Published by CBIORE

control and surface chemistry rather than total surface area alone (Faggiano *et al.,* 2025; Abbaspour *et al.,* 2025).

In this study, biochar was synthesized through pyrolysis at 400°C for 2 hours at atmospheric pressure, based on previously reported optimal conditions (Ariyanti *et al.,* 2025). The novelty of this study lies in the use of mangrove litter as a biochar precursor combined with acid and base activation. CO_2 adsorption on mangrove litter biochar is governed by pore structure and surface functional groups, which are modified through chemical activation. Mangrove litter was selected due to its high organic carbon content and favorable structural properties for carbon sequestration. Compared with commonly studied residues, mangrove litter offers a structurally heterogeneous and carbon-rich precursor that can yield biochar with distinct pore development behavior and surface chemistry upon chemical activation (Ariyanti *et al.,* 2025; Duan *et al.,* 2021; Fernandes *et al.,* 2025; Jayakumar *et al.,* 2023; Kumar *et al.,* 2023; Naseem *et al.,* 2024). Previous studies have also reported that mangrove litter biochar activated with 0.1M HCl is effective for CO_2 adsorption (Ariyanti *et al.,* 2025).

Acid activation using H_2SO_4 and HCl were selected to promote surface functionalization and mineral leaching, whereas KOH and NaOH were used to induce pore modification and introduce basic surface sites, enabling a comparative assessment of acid versus base activation pathways (Choi *et al.,* 2024; Kapoor *et al.,* 2025). The chemically activated biochar was applied as a CO_2 adsorbent, and the adsorption capacity was determined using a static batch CO_2 adsorption method based on changes in CO_2 concentration before and after adsorption (Ariyanti *et al.,* 2025).

This research supports sustainable development in tropical and coastal regions through the utilization of mangrove litter as a biochar feedstock, with the potential to enhance carbon sequestration and reduce atmospheric CO_2, contributing to climate change mitigation and SDGs 13. The specific objectives are to evaluate the effects of activator types (H_2SO_4, HCl, KOH, and NaOH) on the physicochemical characteristics of mangrove litter biochar using SEM-EDX, BET-BJH, FTIR, and CHN analysis, and to determine its CO_2 adsorption capacity as a carbon capture material.

2. Materials and Methods

2.1 Materials

Mangrove litter *(Avicenna marina sp)*, was used as the raw material for biochar production, consisting of twigs and stems collected from the Tapak Mangrove Forest, Tugurejo, Tugu District, Semarang City, Indonesia. The litter was collected during the dry season to minimize moisture variation, and only naturally fallen material was selected to ensure compositional consistency. For chemical activation, analytical grade reagents were used: H_2SO_4 (96-98%, Indrasari, Indonesia), HCl (37%, Supelco-Merck, Sigma-Aldrich), KOH (Indrasari, Indonesia), NaOH (Merck, Germany) and distilled water.

2.2 Methods

2.2.1 Biochar Synthesis

Biomass in the form of mangrove litter was collected and cleaned to remove dirt. The litter was then cut and dried at 105°C in an oven until an equilibrium weight was achieved, as confirmed by three consecutive weight measurements. The dried biomass was then pyrolyzed in a batch fixed-bed reactor

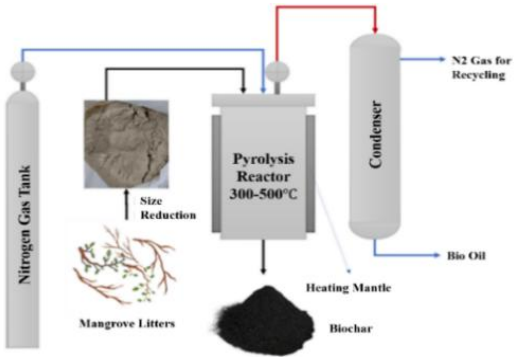

Fig 1 Pyrolysis Scheme

at a heating rate of 10°C min^{-1} to 400°C, where it was maintained for 2 hours under a continuous nitrogen flow of 100 mL min^{-1} to minimize the presence of oxygen during the process. After pyrolysis, the resulting biochar was cooled in a desiccator to prevent oxidation. The schematic of the pyrolysis process is shown in Figure 1.

2.2.2 Biochar Activation

The pyrolyzed biochar was finely ground and sieved using a 50-mesh sieve. Chemical activation was carried out by treating the biochar with 0.1 M H_2SO_4 (B-H_2SO_4); 0.1 M HCl (B-HCl); 0.1 M KOH (B-KOH); and 0.1 M NaOH (B-NaOH) solutions at a biochar-to-solution ratio of 1 g : 4 mL for 2 hours at room temperature. The activator concentration of 0.1 M was selected based on previous studies, which reported effective surface modification without excessive structural degradation of the biochar (Ariyanti et al., 2025). After activation, the samples were filtered using a vacuum pump and repeatedly washed with distilled water until a neutral pH was achieved. The chemically activated biochar (CAB) was then dried at 105°C until it reached a constant weight. Non-activated biochar was prepared as a control sample (B-Control) for comparison.

2.2.3 Biochar Characterization

Characterization was carried out using several methods, Surface morphology and elemental composition were analysed by SEM-EDX. The specific surface area and pore structure were determined by N_2 adsorption-desorption using the BET-BJH methods, respectively. Prior to BET analysis, samples were degassed at 300°C for 3 h, and BET calculations were conducted in the relative pressure (P/P_0) range of 0.004 – 1.00. Functional groups were identified using FTIR in the range of 4000-400 cm^{-1}. Elemental composition (C, H, and N) was determined using a CHN analyser, and the CO_2 adsorption capacity was evaluated by a static batch method.

2.2.4 CO_2 Adsorption

Biochar obtained from pyrolysis was applied as a CO_2 adsorbent using a static batch CO_2 adsorption test box. Prior to adsorption, the system was calibrated until a stable background CO_2 concentration was obtained. A total of 1 g of biochar was placed inside the adsorption box, which was then sealed to prevent gas leakage. CO_2 gas was introduced at a controlled flow rate of 100 mL min^{-1} until the initial CO_2 concentration reached approximately 80-85 mmol CO_2. The adsorption process was conducted at ambient temperature and pressure for 12 h. The CO_2 concentration inside the box was continuously recorded

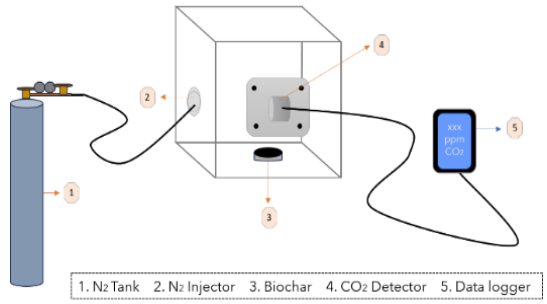

Fig 2 Static Batch CO_2 Adsorption Scheme

using a data logger, and adsorption equilibrium was assumed at the point of maximum CO_2 uptake, defined as the moment immediately before the onset of desorption. The schematic diagram of the static batch CO_2 adsorption test box is presented in Figure 2.

The adsorption capacity was calculated based on the difference between the initial and final CO_2 concentrations and expressed in mmol CO_2 g^{-1} biochar. This method represents a non-isothermal static batch adsorption approach, which has been widely used as a screening technique for evaluating the CO_2 adsorption performance of biochar-based adsorbents under ambient conditions (Ringsby et al., 2024).

3. Results and Discussions

3.1 Characterization of Biochar

3.1.1 SEM-EDX

SEM analysis was employed to determine the surface structure of the CAB samples. Figure 3 displays the images of the control and CAB samples, all of which illustrate irregular surface morphologies. In B-Control, the structure exhibited an uneven and relatively smooth surface with a fragmented pore structure. Following activation with acids (0.1 M H_2SO_4; 0.1 M HCl) and bases (0.1 M KOH; 0.1 M NaOH), the biochar showed a rougher surface morphology with a higher density of visible macropores distributed across the surface. The development of these pores in the CAB structure is expected to enhance the biochar's surface area by providing access to the internal framework.

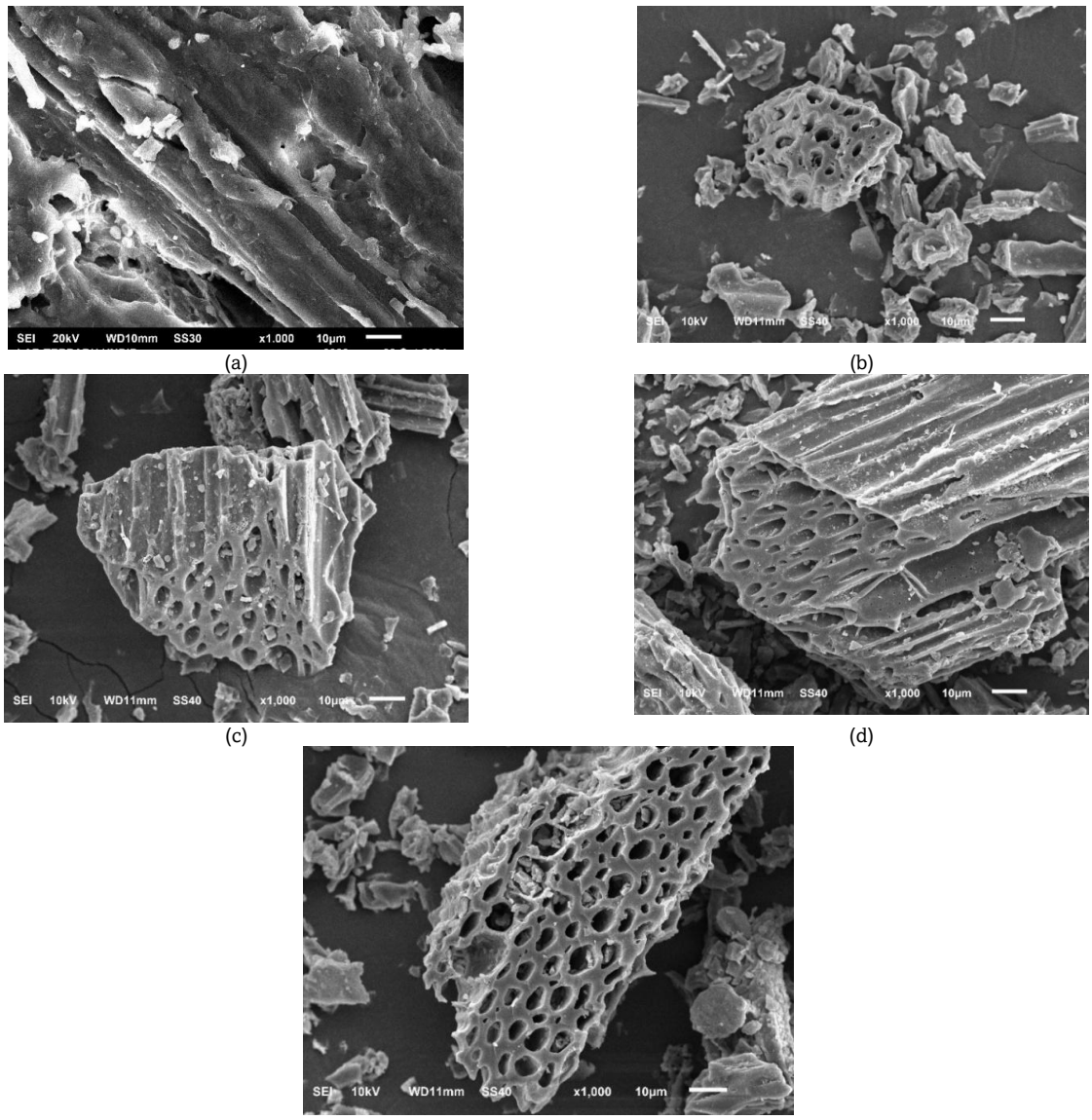

Fig 3 Morphological Analysis of the Chemically Activated Biochar (CAB) (a) B-Control; (b) B-H2SO4; (c) B-HCl; (d) B-KOH; (e) B-NaOH

Table 1
Surface Pore Size Distribution Obtained from SEM Analysis

Sample	Mean Diameter (nm)	Biochar Surface Pore Size Category
B-Control	65,090 ± 45,310	Macropore
B-H_2SO_4	30,810 ± 1,310	Macropore
B-HCl	52,960 ± 29,200	Macropore
B-KOH	61,930 ± 34,260	Macropore
B-NaOH	54,870 ± 1,820	Macropore

Table 2
Surface Elemental Composition Obtained from EDX Analysis

Element (Mass %)	Sample				
	BC	B-H_2SO_4	B-HCl	B-KOH	B-NaOH
C	55.46	31.39	16.68	30.99	31.54
O	42.43	65.23	36.20	48.62	53.53
Na	0.54	0.47	-	1.85	1.99
Mg	0.15	0.72	0.02	3.30	2.03
Cl	0.57	-	0.94	0.34	0.43
K	0.44	1.81	6.03	9.74	0.42
Ca	0.29	-	8.04	5.16	9.24
Fe	-	0.37	32.09	-	1.83

This morphological transformation is comparable to the findings of Ahuekwe *et al.,* (2025), where pyrolysis and chemical modification were reported to shift the surface from a near-smooth, non-porous state to a densely packed, porous structure. Furthermore, the increased roughness observed in CAB aligns with the observations of Monteagudo et al., (2025), who achieved significant corrosion and micropore creation using a high-temperature activation (750°C). These results demonstrate that even at a lower activator concentration and milder conditions, the mangrove-derived biochar still exhibits a distinct irregular and heterogeneous surface morphology. Table 1 presents the pore size categories for the biochar surfaces. Based on IUPAC classification, the pore sizes observed by SEM fall within the macropore range (>50 nm). These macroporous structures function as gas diffusion pathways.

The elemental composition of the biochar samples was analysed using EDX, showing carbon (C) and oxygen (O) as the dominant elements, with minor contributions from Na, Mg, Cl, K, Ca, and Fe as shown in Table 2. Compared to the B-Control (55.46 wt% C and 42.43 wt% O), all chemically activated samples exhibited a decrease in carbon content and an increase in oxygen content. The most pronounced changes were observed in acid-activated biochars, particularly B-H_2SO_4, where carbon decreased to 31.39 wt% (ΔC=−24.07 wt%) and oxygen increased to 65.23 wt% (ΔO=+22.80 wt%). Similarly, B-HCl showed a substantial reduction in carbon to 16.68 wt% (ΔC=−38.78 wt%) and an oxygen content of 36.20 wt% (ΔO=−6.23 wt%), indicating extensive surface modification during acid treatment. Activation with strong acids such as H_2SO_4 can oxidize biochar, resulting in the generation of more oxygen-containing functional groups. This process increases the oxygen content while potentially removing some carbon through the formation of volatile organic compounds (Baharim *et al.,* 2023; Sivaraman *et al.,* 2025; Song *et al.,* 2024). Acid treatment also enhances the surface functionalization of biochar, leading to an increase in oxygen content due to the presence of acidic functional groups (Baharim *et al.,* 2023; Song *et al.,* 2024).

Regarding alkali-acyivated biochars, B-KOH and B-NaOH exhibited carbon contents of 30.99 wt% and 31.54 wt%, respectively, corresponding to reductions of 24.47 wt% and 23.92 wt% relative to B-Control, while their oxygen contents increased to 48.62 wt% (ΔO=+6.19 wt%) and 55.33 wt% (ΔO=+12.90 wt%). These trends are consistent with the reaction of alkali agents with carbon in biochar, producing gaseous products such as CO_2 and CO. This reaction reduces the carbon content in the biochar (Chen *et al.,* 2020; M & Gupta, 2025; Premchand *et al.,* 2024). Alkali also react with oxygen-containing species in biochar, resulting in the formation of new oxygen-containing functional groups such as hydroxyl (-OH), carbonyl (C=O), and carboxyl (-COOH) groups. This increases the oxygen content in the biochar (Chen *et al.,* 2020; Liu *et al.,* 2024; M & Gupta, 2025).

In addition to changes in C and O, the presence of inorganic elements reflects the influence of the activating agents. For instance, the enrichment of K in B-KOH (9.74 wt%) and Na in B-NaOH (1.99 wt%) indicates residual alkali species or their reaction products on the biochar surface, which may enhance cation exchange capacity and alter surface morphology (Bentley *et al.,* 2022; Yan *et al.,* 2024). The occurrence of MgO-related species, as suggested by the Mg content, may contribute to particle aggregation within or on the surface of the biochar (Bentley *et al.,* 2022; Yan *et al.,* 2024).

3.1.2 BET-BJH

The surface area and pore size of biochar were characterized using the Brunauer-Emmett-Teller (BET) and Barret-Joyner-Halenda (BJH) methods. Table 3 presents the spesific surface area (SSA), average pore width, total pore volume, and micropore volume of the biochar samples. Micropores are defined as pores with a diameter of less than 2 nm, mesopores range from 2–50 nm, and macropores have a diameter of more than 50 nm (Ariyanti et al., 2024). Based on the average pore width values, all biochar samples exhibit microporous characteristics (<2 nm), indicating that micropores are the dominant pore structure across all samples. Chemical activation significantly increased the specific surface area and micropore volume compared to the control biochar. This enhancement is attributed to the release of gases (H_2, CO, and CO) during the activation process, which enlarges existing pores and generates new micropores within the carbon matrix (Qu et al., 2021). The highest micropore volume was observed in B-KOH, indicating that KOH activation was the most effective in developing microporous structures among all samples. A high micropore

Table 3
Elemental BET Specific Area (SSA), Average Pore Width (Dpore), Total Pore Volume (Vtotal), and V Micropore

Sample	Surface Area (m^2/g)	Average Pore Width (nm)	Total Pore Volume (cm^3/g)	Micropore Volume (cm^3/g)
B-Control	72.149	1.688	0.05	0.001749
B-H_2SO_4	211.124	1.614	0.01494	0.004586
B-HCl	184.068	1.614	0.03037	0.004836
B-KOH	195.896	1.543	0.03546	0.005927
B-NaOH	192.348	1.614	0.01098	0.0045

content is known to enhance CO_2 adsorption capacity, as micropore volume is a key controlling factor in CO_2 uptake by carbonaceous adsorbents (J. Zhang *et al.,* 2020). In this study, the highest micropore content was found in KOH-activated biochar.

A high micropore content can increase CO_2 adsorption capacity. This finding aligns with research by J. Zhang *et al.,* (2020) that found that micropore volume is a key factor in CO_2 adsorption capacity in activated biochar. In this study, the highest micropore content was found in KOH-activated biochar. Figure 4 illustrates the N_2 adsorption/desorption isotherms of mangrove biochar. All samples were degassed at 300°C for 3 hours to ensure the removal of surface impurities. The N_2 adsorption-desorption isotherms exhibit a combination of Type

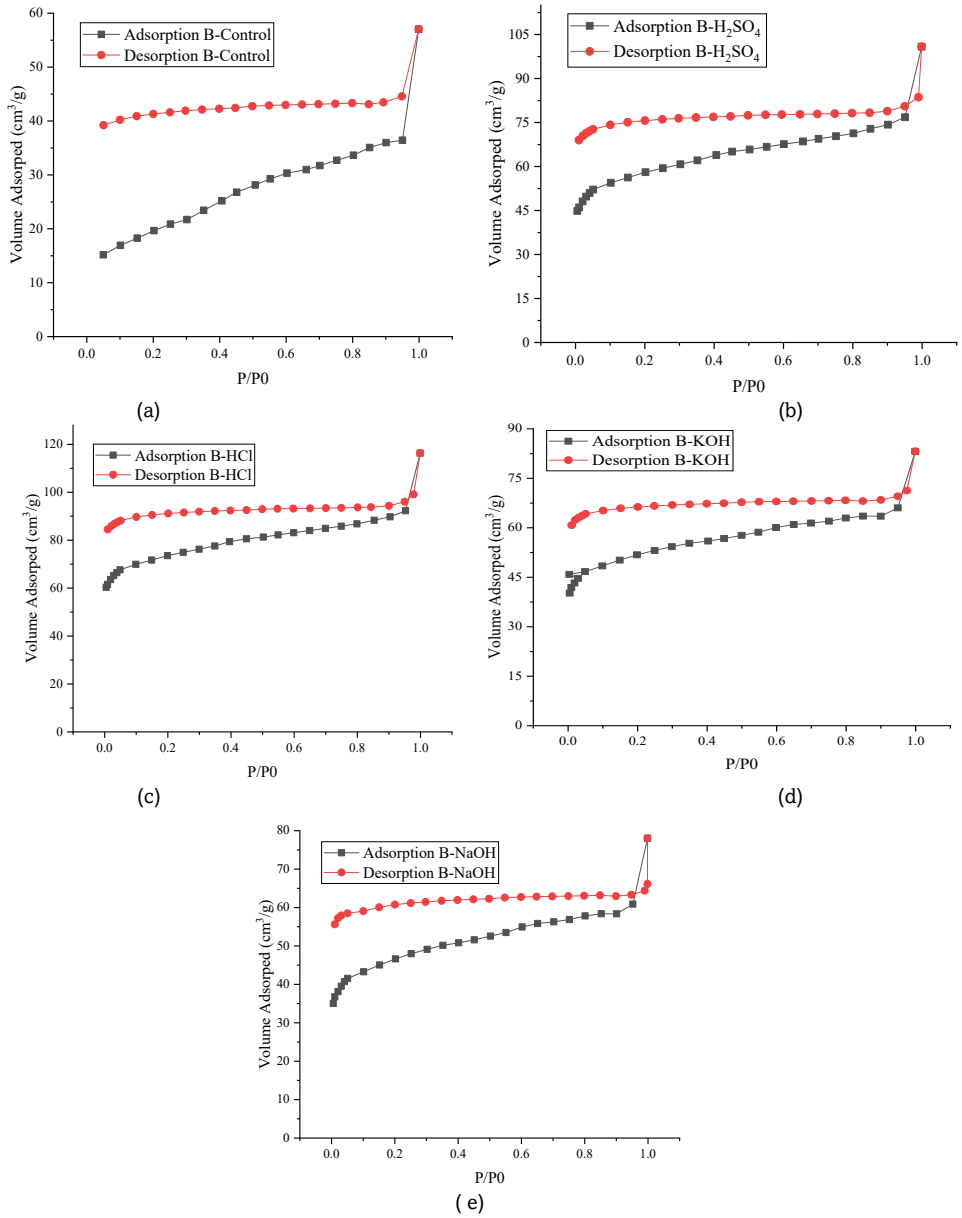

Fig 4 N_2 Adsorption and Desorption Isotherm (a) B-Control; (b) B-H2SO4); (c) B-HCl; (d) B-KOH; (e) B-NaOH

I and Type IV characteristics according to IUPAC classification. The sharp volume uptake at P/P0 < 0.1 confirms the presence of micropores (Type I), while the hysteresis loop at medium pressure indicates mesoporosity (Type IV) (Wang et al., 2023). The hysteresis loops are identified as Type H4, reflecting a slit-like pore structure. The hysteresis phenomenon is clearly visible in all samples, characterized by a gap between the adsorption and desorption curves (Peng *et al.,* 2023). This occurrence can be caused by various factors, mainly involving changes in the physical structure of the material and the presence of impurities on the biochar surface (Feng *et al.,* 2024; Li *et al.,* 2025). Quantitative data in Table 3 supports these findings, with average pore widths ranging from 1.543 nm to 1.688 nm, which strictly fall within the micropore category (<2 nm).

3.1.3 FTIR

The FTIR spectrum shown in Figure 5 demonstrates changes in the intensity and presence of functional groups following pyrolysis and chemical activation. As mangrove biomass is a heterogeneous material, numerous characteristic peaks are observed (Rahman *et al.,* 2023). Functional groups that were initially dominant in the raw mangrove biomass underwent degradation, weakening, or structural rearrangement depending on the type of activator used as shows in Table 4. In the raw mangrove biomass, a broad peak around 3250–3650 cm^{-1} is attributed to O-H stretching, representing hydrogen-bonded water, alcohol, and carboxylic acid (Nandiyanto *et al.,* 2023). However, this peak weakened considerably in the biochar samples after pyrolysis and chemical activation. This trend indicates that the hydroxyl groups underwent thermal degradation and decomposed into volatile compounds during pyrolysis at 400°C (Ahuekwe *et al.,* 2025). This observation is analytically consistent with the findings of Ahuekwe *et al.,* (2025), who reported that the near-total disappearance of the -OH stretching vibration is a hallmark of successful carbonization. While Ahuekwe *et al.,* (2025) observed this transition during the shift from raw biomass to biochar at similar temperatures, our results further show that chemical activation accelerates the removal of these polar groups compared to the B-Control. This suggests that the activators in our study not only facilitated carbonization but also promoted the dehydration of the mangrove's lignocellulosic framework more effectively than thermal treatment alone. The reduction of these hydrophilic groups is crucial for CO_2 adsorption, as it potentially increases the surface hydrophobicity, thereby reducing moisture interference during gas capture.

C-H stretching between 2800 – 3000 cm^{-1} indicate aliphatic hydrocarbons present in all samples (Nandiyanto *et al.,* 2023), but their intensity decreases compared to that in mangrove biomass, indicating partial decomposition of the aliphatic chains of cellulose and hemicellulose compounds. Acid (H_2SO_4, HCl) and base (KOH, NaOH) activation did not completely remove the C-H functional groups. In the range 1580–1630 cm^{-1}, indicate C=C peaks and some C=O peaks (Nandiyanto *et al.,* 2023). These peaks appear in all samples with varying intensity. In mangrove biomass, these peaks represent the carbonyl groups of carboxylic acids and aldehydes (Nandiyanto *et al.,* 2023). After pyrolysis, the peak shifts to the range 1581–1595 cm^{-1}, indicating the transformation of polar groups into stable aromatic structures through decarboxylation and aromatic condensation (Birhanu *et al.,* 2025). Base and acid activation do not remove these groups but instead strengthen the aromatic structure through dehydrogenation.

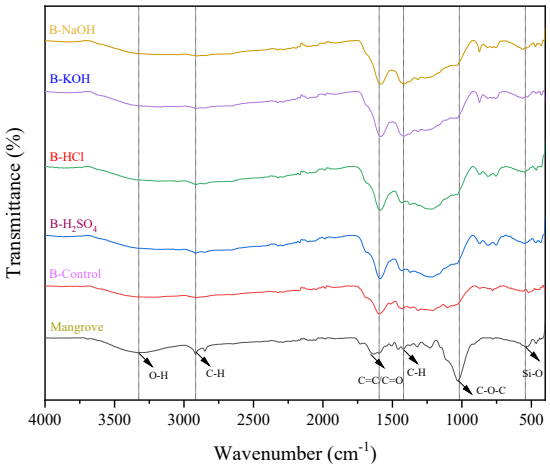

Fig 5 Functional Groups Spectrum of the Chemically Activated Biochar (CAB)

The C-H group appearing between 1416 and 1420 cm^{-1} indicates the presence of an aliphatic methylene chain (Nandiyanto *et al.,* 2023). This group still appears after pyrolysis, but with reduced intensity. This change indicates that some of the aliphatic structure remains in a carbonized form and not entirely decomposed into aromatics. Base activation showed a slight improve in this group compared to the B-Control. The C–O–C (eter) peak was clearly detected in mangrove biomass, indicating a lignocellulosic structure rich in polar compounds (Nandiyanto *et al.,* 2023). After pyrolysis, this peak weakened or shifted, indicating the cleavage of glycosidic bonds and fragmentation of the eter structure (Birhanu *et al.,* 2025). Base activation generally causes the disappearance of this group, indicating the ability of strong bases to hydrolyze C–O bonds. Absorption bands under 600 cm^{-1} correspond to Si–O–Si vibrations originating from ash and natural minerals in the biomass (Nandiyanto *et al.,* 2023). These peaks persisted in all samples, indicating that the inorganic components were neither dissolved by activation nor degraded by heat, thus contributing to the stability of the final biochar structure.

Table 4

The Effect of Chemically Activated Biochar (CAB) on Functional Groups

Functional Group	Wavelength (cm^{-1})					
	M	BC	B-H_2SO_4	B-HCl	B-KOH	B-NaOH
O-H	3328	3342	3344	3342	3330	3333
C-H	2916	2908	2920	2914	2910	2908
C=C	1639	1595	1589	1583	1582	1583
C=O	1228	1207	1217	1224	1419	1419
C-H	-	778	872	870	873	871
C-O-C	1028	-	-	-	-	-
Si-O-Si	545	515	547	546	560	569

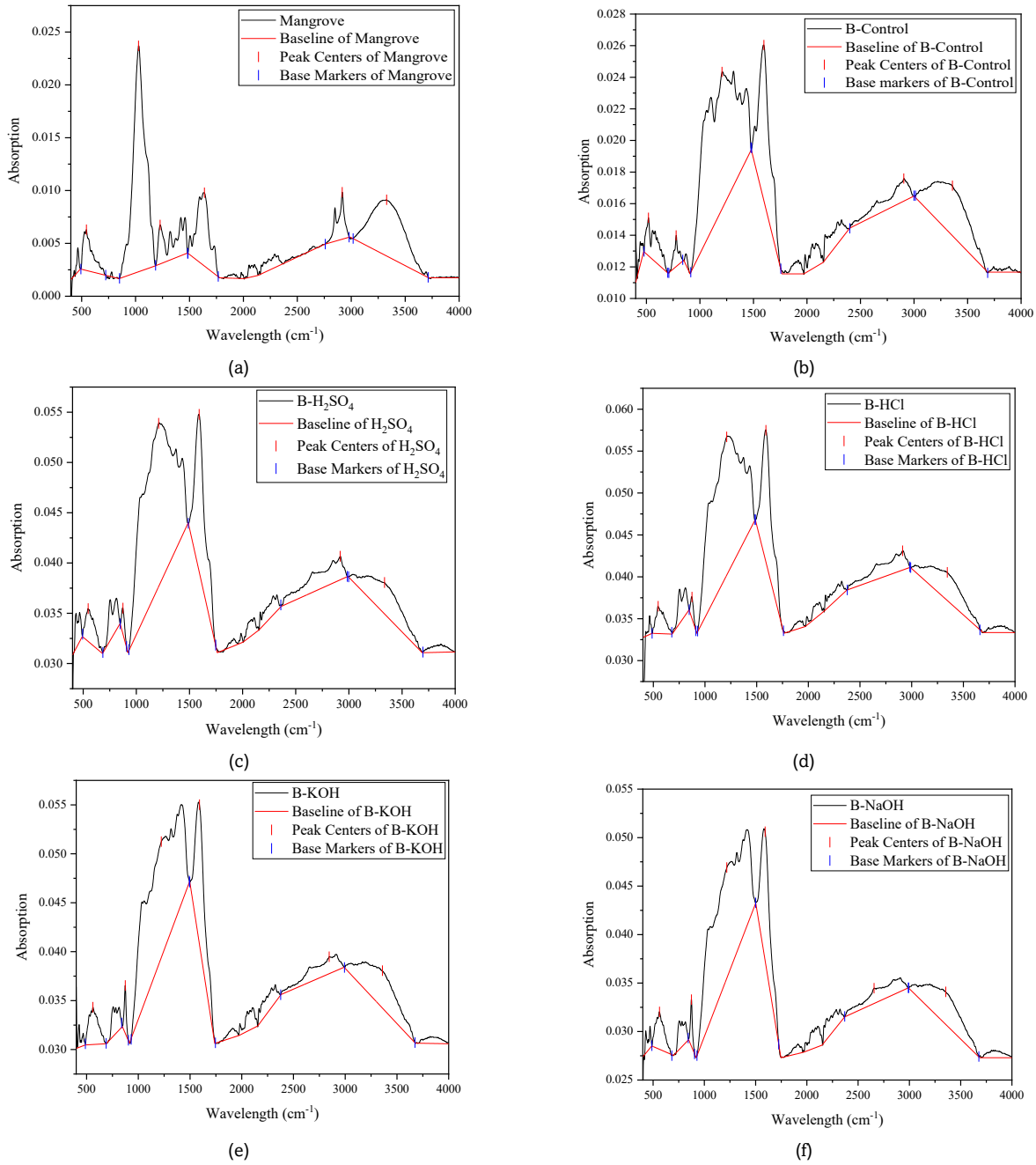

Fig 6 The Effect of Chemically Activated Biochar (CAB) on Area Functional Group

Table 5
The Effect of Chemically Activated Biochar (CAB) on Total Peak Area

Functional Group	Peak Area (a.u. x cm^{-1})					
	M	BC	B-H_2SO_4	B-HCl	B-KOH	B-NaOH
O-H	1,906	1,242	1,223	1,299	1,533	1,906
C-H	0,329	0,371	0,822	0,739	0,573	0,329
C=C	0,961	1,198	1,742	1,751	1,513	0,961
C=O	0,612	3,276	5,853	5,899	4,955	0,612
C-O-C	2,865	-	-	-	-	2,865
C-H	-	0,093	0,080	0,081	0,109	-
Si-O-Si	0,383	0,269	0,226	0,319	0,406	0,383
Total Peak Area	7,056	6,449	10,056	10,087	9,089	7,056

The functional group area of mangrove biomass, control biochar, and CAB is shown in Figure 6 and Table 5. There was a decrease in the functional group area in control biochar compared with mangrove biomass, indicating that the pyrolysis process at 400°C for 2 hours resulted the loss of volatile groups from the biochar. After chemical activation, the functional group

area of the biochar increased compared with B-Control. This increase is commonly attributed to surface oxidation and structural rearrangement during activation, which can generate or expose new active oxygen-containing functional groups on the carbon surface (Xie *et al*., 2025; Birhanu *et al*., 2025). The functional group area can be an indicator of CO_2 adsorption capacity, Because the presence of polar groups, including hydroxyl (–OH) and carbonyl (–CO) have the ability to interact with CO_2 molecules through electrostatic and hydrogen bonds (Xie *et al.,* 2025). However, this factor is not always directly proportional to the adsorption capacity. The CO_2 adsorption capacities of biochar are more dominantly controlled by the volume and distribution of micropores. Polar functional groups increase chemical interactions with CO_2.

3.1.4 CHNS

The elemental content was detected with CHNS/O Analyser. Table 6 shows the elemental composition of biochar. The most basic and essential element is C, also generally the highest (Hameed *et al.,* 2024). In this study, the percentage of C was the highest of all elements and increased in acid-activated (H_2SO_4, HCl) and base-activated (KOH, NaOH) biochar compared to the control biochar. This carbon enrichment aligns with the findings of Alcazar-Ruiz *et al.,* (2024), who stated that chemical activation promotes the removal of non-carbonaceous compounds to enrich the carbon framework, that excessive KOH activation could potentially decrease the carbon fraction. This result demonstrates that 0.1M concentration used successfully maintain the aromatic structural stability. This indicates that there is potential for CAB for adsorption activity (Monteagudo *et al.,* 2025). The percentage of O tended to decrease from the control biochar, this likely occurred due to the washing process after activation which resulted in the loss of non-carbon soluble compounds and unreacted activator residues attached to the biochar surface (Bakshi *et al.,* 2020). As research from Monteagudo *et al.,* (2025) found that the washing process using H_2O and HCl resulted in a decrease in the O content in biochar. Meanwhile, H, although small, generally accounts for 1%-3% of the total biochar mass. H is an important active component, such as hydrogen bonds and active functional groups (Xiao *et al.,* 2018). The increased N concentration indicates that CAB receives additional functional groups from the activator, potentially enhancing CO_2 uptake through chemisorption (Zhang *et al.,* 2023).

Aromaticity and polarity through the H/C and (N+O)/C ratios (Bakshi *et al.,* 2020). A higher (N+O)/C ratio implies enrichment of polar functional groups, which can improve the biochar's affinity for polar molecules such as CO_2 and water (Bakshi *et al.,* 2020). The O/C atomic ratio decreased in CAB compared to the control biochar, indicating an increase in aromatic structure in CAB (X. Liu *et al.,* 2022; Q. W. Li *et al.,* 2021). Carbon stability in biochar is reflected in the H/C molar ratio, where a low H/C value correlates with increased carbon stability (Adhikari *et al.,* 2024). Based on the International Biochar Initiative (Standardized Product Definition and Product Testing Guidelines for Biochar That Is Used in Soil (Aka IBI Biochar Standards), n.d.) standards, high-quality biochar It is required to exhibit an H/C ratio below 0.7. The H/C values in this study met this standard for all samples. A high N/C ratio indicates sufficient nitrogen content, which can also increase adsorption capacity through the formation of active nitrogen sites (Zhang *et al*., 2024). The biochar produced in this study is classified as class 1 because it has a carbon content above 60%(Standardized Product Definition and Product Testing Guidelines for Biochar That Is Used in Soil (Aka IBI Biochar Standards), n.d.; Yadav *et al.,* 2023).

2.2 CO_2 Adsorption

The CO_2 adsorption capacities were measured using a static batch CO_2 Adsorption test box for 12 hours using B-Control and CAB. Figure 7 shows the CO_2 adsorption profiles of the biochar samples. Among the samples, B-Control exhibited the lowest adsorption capacity (5.65 mmol/g), while B-KOH showed the highest adsorption capacity (12.47 mmol/g). The other chemically activated biochars (B-HCl, B-H_2SO_4, and B-NaOH) also showed higher adsorption capacities than the control biochar, following a similar trend.

CO_2 adsorption capacity can be enhaned through surface and pore structure modification, such as acid-base activation (Bhattacharjee *et al.,* 2025). The CO_2 capture mechanism by biochar involves both physical and chemical adsorption processes (Long *et al.,* 2025). Physical adsorption is governed by van der Waals forces and pore filling, whereas chemical adsorption involves Lewis acid-base interactions and hydrogen bonding between CO2 and surface functional groups (Bhattacharjee *et al.,* 2025; Quan *et al.,* 2023).

Chemical activation using KOH significantly increased the CO_2 adsorption capacity, which is closely related to the development of microporosity and surface chemistry of the biochar (Alcazar-Ruiz *et al*., 2024). KOH activation is widely reported to be more effective than physical activation in enhancing CO2 adsorption performance due to its strong pore-forming (porogenic) effect and its ability to intercalate into the carbon matrix during activation (Alcazar-Ruiz *et al.,* 2024).

The redox reaction between KOH and the carbon material resulted in an increase in potassium (K) content in the biochar (Komatsu *et al.,* 2022), with EDX characterization results showing the highest K content in KOH-activated biochar (B-KOH), at 9.74%. Rather than evaporating and directly bonding to carbon sites, potassium primarily acts as a porogen and intercalation agent that penetrates the carbon matrix, enlarges existing pores, and promotes pore structure development

Table 6
The Effect of Chemically Activation Biochar (CAB) on Elemental Composition and Ratio

Sample	BC	B-H_2SO_4	B-HCl	B-KOH	B-NaOH
C	64.32	73.40	73.69	70.33	70.39
H	4.764	4.383	4.504	4.22	4.351
N	0.97	1.45	1.44	1.35	1.38
S	0.048	0.169	0.513	0.068	0.071
O[a]	29.898	20.598	19.853	23.868	23.808
H/C	0.074	0.059	0.061	0.06	0.062
O/C	0.465	0.281	0.269	0.339	0.338
N/C	0.015	0.0197	0.0195	0.0192	0.0196
(N+O)/C	0.479	0.3	0.289	0.359	0.358

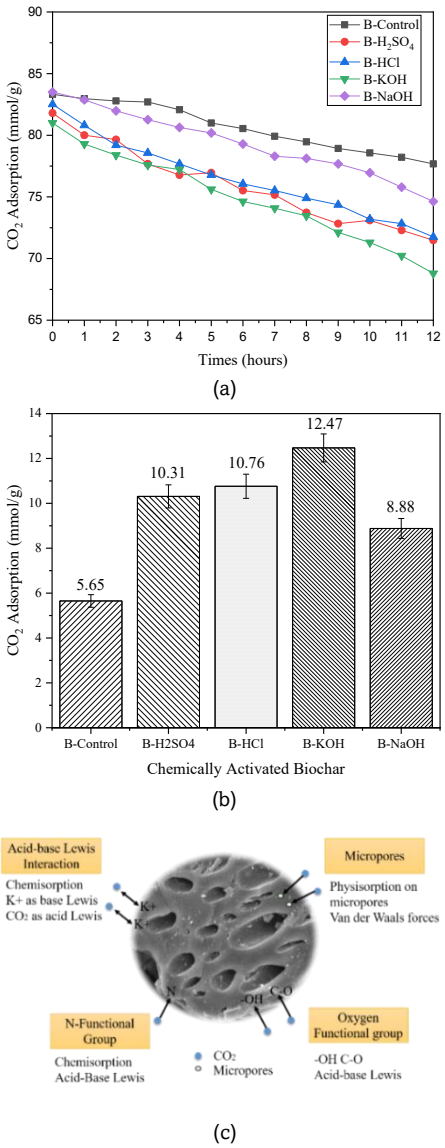

Fig 7 Chemically Activated biochar (CAB) profile on CO_2 adsorption (a) adsorption profile by the time; (b) adsorption capacity; (c) proposed mechanism. Adapted with permission from *(Amer et al., 2024)*

through carbon lattice expansion and gasification reactions (Komatsu *et al.,* 2022; J. Liu *et al.*, 2022). As a result, B-KOH exhibited the highest micropore volume among the samples (5.927×10^{-3} cm^3 g^{-1} based on BET analysis). Although this micropore volume is lower than that of highly activated commercial carbons, it is relatively higher within the set of biochars investigated in this study and is sufficient to explain the observed enhancement in CO_2 adsorption.

The weakly acidic property of CO_2 enables the enhancement of its adsorption capacity when basic Lewis sites, such as K^+ ions, are introduced onto the carbon surface (Ma *et al.*, 2025). his improvement is attributed to chemisorption interactions between CO_2 molecules and the adsorbent, where hydrogen bonding is established with –OH groups formed during KOH activation (Freyre *et al.,* 2023). Supporting evidence is seen from the FTIR characterization results, which show that the –OH group area in KOH-activated biochar is larger than in other activated biochar. Further analysis revealed that these hydrogen bonds can lower the bond the interaction energy between the adsorbent and CO_2, thus improving the overall CO_2 adsorption capacity (Long *et al.,* 2025; Quan *et al.,* 2023).

The capacity of CO_2 adsorption activated biochar is also affected by an elevated (N+O)/C ratio, which reflects the abundance of polar functional groups and thereby enhances its interaction with polar molecules like CO_2 and water. Meanwhile, a lower O/C atomic ratio signifies greater stability of the aromatic framework within the activated biochar (Li *et al.,* 2021). The stability of carbon in biochar is reflected in the H/C molar ratio, where a low H/C value correlates with increased carbon stability. These factors positively influence CO_2 adsorption (Alcazar-Ruiz *et al.,* 2024).

The CO_2 adsorption mechanism is governed not by a single parameter, but by the combined influence of multiple factors, such as elemental composition, functional groups, pore structure, and surface chemical characteristics, including acidity, hydrophilicity, and polarity of the activated biochar (Igalavithana *et al.,* 2020). Based on the BET results, micropore filling is identified as the dominant mechanism, as the narrow micropores (< 2 nm) provide strong adsorption potential due to overlapping adsorption fields. KOH activation promotes the development of a well-defined microporous structure, increasing the number of available adsorption sites. SEM analysis reveals the presence of microporous, which act as transport channels facilitating CO_2 diffusion toward internal micropores where adsorption predominantly occurs. In addition, FTIR analysis confirms the presence of oxygen-containing functional groups that enhance CO2-surface interactions, while CHN results indicate surface polarity and aromaticity that further contribute to adsorption capacity. Thus, the results showed that the CO_2 adsorption capacity of all activated biochar samples tested followed the order KOH > HCl > H_2SO_4 > NaOH > Control. Therefore, the best activator is KOH which produces a more microporous structure and has superior adsorption properties.

4. Conclusion

A study of acid and base-activated biochar derived from mangroves demonstrated its interesting function in carbon sequestration. The results showed that chemical activation of biochar significantly increased CO_2 adsorption capacity compared to non-activated biochar (B-Control). Of all the activation types tested, KOH was the most effective activator, producing the highest capacity of 12.47 mmol/g. This increase was due to the formation of a wide micropore distribution, high potassium (K) content, and due to the existence of polar groups, for instance –OH that strengthen the chemisorption interaction through hydrogen bonds and Lewis acid-base interactions with CO_2 molecules. Characterization showed that KOH-activated biochar had the highest K content (9.74%), the largest micropore volume (5.927×10^{-3} cm^3/g). In addition, the stability of the aromatic structure and hydrophilic properties also supported the increase in adsorption. The CO_2 adsorption mechanism involves a synergy between pore structure, elemental composition, functional groups and surface characteristics, including polarity and acidity. The order of activation effectiveness in increasing CO_2 adsorption is: KOH > HCl > H_2SO_4 > NaOH > Control.

Acknowledgments

The authors acknowledged the Faculty of Engineering, Universitas Diponegoro for the financial support No:

91/UN7.F3/HK/IV/2025 and Universitas Diponegoro World Class University Visiting Professor Program of 2025.

Author Contributions: DA: Conceptualization, methodology, supervision, analysis, writing—original draft-review, VS: material preparation, data collection, writing—original draft, project administration, FH: material preparation, data collection, IW: review and editing, WW: review and editing, SS: review and editing, AP: writing-review, validation, HS: review; FH: review. All authors have read and agreed to the published version of the manuscript.

Funding: The author received financial support from the Faculty of Engineering, Universitas Diponegoro No: 91/UN7.F3/HK/IV/2025 and Universitas Diponegoro World Class University Visiting Professor Program of 2025.

Conflicts of Interest: The authors declare no conflict of interest in conducting research and writing this article. All research results and interpretations are in accordance with actual conditions and there is no intervention from any party.

References

Abbaspour, N., Jordan, C., Tondl, G., Wąsik, P., Gholizadeh, T., Tomasetig, D., Szlęk, A., Pfeifer, C., Harasek, M., Korus, A., & Winter, F. (2025). Activated biochars from heavy metal-contaminated biomass for CO2 capture: Adsorption performance and dominant mechanisms. *Journal of CO2 Utilization*, *101*, 103217. https://doi.org/10.1016/J.JCOU.2025.103217

Adhikari, S., Moon, E., Paz-Ferreiro, J., & Timms, W. (2024). Comparative analysis of biochar carbon stability methods and implications for carbon credits. *Science of the Total Environment*, *914*. https://doi.org/10.1016/j.scitotenv.2023.169607

Agency EP. (2022). *Climate Change Indicator: Atmospheric Concentrations of Greenhouse Gases*. Climate Change Indicators: Atmospheric Concentrations of Greenhouse Gases | US EPA

Ahuekwe, E. F., Abimbola, B. S., Agwamba, E. C., & Durodola, B. (2025). Characterisation of pristine and KOH-modified rice husk biochars for efficient heavy metal removal in wastewater treatment. *Scientific African*, *28*. https://doi.org/10.1016/j.sciaf.2025.e02678

Alcazar-Ruiz, A., Maisano, S., Chiodo, V., Urbani, F., Dorado, F., & Sanchez-Silva, L. (2024). Enhancing CO2 capture performance through activation of olive pomace biochar: A comparative study of physical and chemical methods. *Sustainable Materials and Technologies*, *42*. https://doi.org/10.1016/j.susmat.2024.e01177

Amalina, F., Razak, A. S. A., Krishnan, S., Sulaiman, H., Zularisam, A. W., & Nasrullah, M. (2022). Biochar production techniques utilizing biomass waste-derived materials and environmental applications – A review. In *Journal of Hazardous Materials Advances* (Vol. 7). Elsevier B.V. https://doi.org/10.1016/j.hazadv.2022.100134

Amer, N. M., Lohijani, P., Mohammadi, M., & Mohamed, A. R. (2024). Modification of biomass-derived biochar: A practical approach towards development of sustainable CO2 adsorbent. *Biomass Conversion and Biorefinery*, *14*, 7401–7448. https://doi.org/10.1007/s13399-022-02905-3

Ariyanti, D., Nugroho, D., Purbasari, A., Azizah, N. U., Nurwidiyanto, A. R., & Gao, W. (2025). Activated mangrove biochar for sustainable carbon sequestration. *E3S Web of Conferences*, *655*. https://doi.org/10.1051/e3sconf/202565501028

Ariyanti, D., Purbasari, A., Sugianto, D. N., Lesdantina, D., & widiyanti, M. (2024). Rice husk-based magnetic biochar produced via hydrothermal route for petroleum spills adsorption: characterization, adsorption kinetics, and isotherms. *Adsorption*. https://doi.org/10.1007/s10450-024-00544-w

Baharim, N. H., Sjahrir, F., Mohd Taib, R., Idris, N., & Tuan Daud, T. A. (2023). Removal of Crystal Violet from Aqueous Solution using Post-Treated Activation Biochar Derived from Banana Pseudo Stem. *Chemical Engineering Transactions*, *98*, 45–50. https://doi.org/10.3303/CET2398008

Bakshi, S., Banik, C., & Laird, D. A. (2020). Estimating the organic oxygen content of biochar. *Scientific Reports*, *10*(1). https://doi.org/10.1038/s41598-020-69798-y

Bentley, M. J., Kearns, J. P., Murphy, B. M., & Summers, R. S. (2022). Pre-pyrolysis metal and base addition catalyzes pore development and improves organic micropollutant adsorption to pine biochar. *Chemosphere*, *286*. https://doi.org/10.1016/j.chemosphere.2021.131949

Bhattacharjee, N., Jha, A., & Mukherjee, A. (2025). Functionalization of activated carbon to tailor the textural properties and surface functionalities. In *Activated Carbon: Synthesis, Analysis, and Industrial Applications* (pp. 81–102). Elsevier. https://doi.org/10.1016/B978-0-12-821996-6.00008-7

Birhanu, A., Hailu, A. M., Worku, Z., Tessema, I., Angassa, K., & Tibebu, S. (2025). Optimization of pyrolysis conditions for Catha edulis waste-based biochar production using response surface methodology. *Bioresources and Bioprocessing*, *12*(1). https://doi.org/10.1186/s40643-025-00866-9

Chen, W., Gong, M., Li, K., Xia, M., Chen, Z., Xiao, H., Fang, Y., Chen, Y., Yang, H., & Chen, H. (2020). Insight into KOH activation mechanism during biomass pyrolysis: Chemical reactions between O-containing groups and KOH. *Applied Energy*, *278*. https://doi.org/10.1016/j.apenergy.2020.115730

Choi, G., Kan, E., Lee, J. H., & Choi, Y. (2024). Insight into the performance and microbial community of anaerobic digestion treating cow manure with a novel iron-functionalized activated biochar. *Chemosphere*, *364*. https://doi.org/10.1016/j.chemosphere.2024.143058

Deng, L., Wu, C., Fu, L., Wang, Y., An, Q., Liu, G., & Wan, C. (2024). Preparation of biochar and its adsorbing performance evaluation in the petroleum hydrocarbon. *Biomass Conversion and Biorefinery*, *14*(21), 26895–26904. https://doi.org/10.1007/s13399-022-03439-4

Duan, D., Lei, P., Lan, W., Li, T., Zhang, H., Zhong, H., & Pan, K. (2021). Litterfall-derived organic matter enhances mercury methylation in mangrove sediments of South China. *Science of the Total Environment*, *765*. https://doi.org/10.1016/j.scitotenv.2020.142763

Faggiano, A., Cicatelli, A., Guarino, F., Castiglione, S., Proto, A., Fiorentino, A., & Motta, O. (2025). Optimizing CO2 capture: Effects of chemical functionalization on woodchip biochar adsorption performance. *Journal of Environmental Management*, *380*, 125059. https://doi.org/10.1016/J.JENVMAN.2025.125059

Feng, Y., Lin, D., Yang, K., & Wu, W. (2024). Desorption hysteresis of antibiotics on biochar produced at high temperature: The role of amine groups and amidation reaction. *Science of the Total Environment*, *952*. https://doi.org/10.1016/j.scitotenv.2024.175998

Fernandes, J. D., de Souza Laurentino, L. G., Chaves, L. H. G., de Andrade, J. N. F., da Silva, A. A. R., Kubo, G. T. M., de Lima, G. S., & de Lima, A. M. (2025). Different biochar: effects on soil fertility and growth of bell pepper[Diferentes biocarvões: efeitos na fertilidade do solo e no crescimento de pimentão]. *Revista Caatinga*, *38*. https://doi.org/10.1590/1983-21252025v3812730rc

Freyre, P., St. Pierre, E., & Rybolt, T. (2023). Carbon Dioxide Capture by Adsorption in a Model Hydroxy-Modified Graphene Pore. *International Journal of Molecular Sciences*, *24*(14). https://doi.org/10.3390/ijms241411452

Guarin, D., Fernandez, A., Benavides, J., & Rangel, N. (2025). Biochar for climate change mitigation and soil health management. In *Biochar Ecotechnology for Sustainable Agriculture and Environment* (pp. 231–259). Elsevier. https://doi.org/10.1016/B978-0-443-29855-4.00011-4

Hameed, R., Abbas, A., Balooch, S., Khattak Wajid Ali, Nazir, M. M., Naqvi, S., Li, G., & Du, D. (2024). Climate change in interaction with global carbon cycle. In *Challenges and Solutions of Climate Impact on Agriculture* (pp. 227–257). Elsevier. https://doi.org/10.1016/B978-0-443-23707-2.00009-X

Igalavithana, A. D., Choi, S. W., Shang, J., Hanif, A., Dissanayake, P. D., Tsang, D. C. W., Kwon, J. H., Lee, K. B., & Ok, Y. S. (2020). Carbon dioxide capture in biochar produced from pine sawdust and paper mill sludge: Effect of porous structure and surface chemistry.

Science of the Total Environment, *739*. https://doi.org/10.1016/j.scitotenv.2020.139845

Jayakumar, M., Hamda, A. S., Abo, L. D., Daba, B. J., Venkatesa Prabhu, S., Rangaraju, M., Jabesa, A., Periyasamy, S., Suresh, S., & Baskar, G. (2023). Comprehensive review on lignocellulosic biomass derived biochar production, characterization, utilization and applications. *Chemosphere*, *345*. https://doi.org/10.1016/j.chemosphere.2023.140515

Kapoor, R. T., Rafatullah, M., Siddiqui, M. R., & Alam, M. (2025). Sequestration of reactive blue 19 dye by nitrogen-doped palm kernel shell biochar: Kinetics, thermodynamics, regeneration potential and phytotoxicity studies. *Journal of the Indian Chemical Society*, *102*(6). https://doi.org/10.1016/j.jics.2025.101749

Komatsu, K., Watanabe, T., Tsuda, Y., & Saitoh, H. (2022). Preparation of Nanoporous Carbon from Rice Husk through Alkali Activation Treatment: a Detailed Mechanistic Investigation. *Silicon*, *14*(14), 9117–9127. https://doi.org/10.1007/s12633-021-01619-x

Kumar, A., Kumari, M., Azim, U., Vithanage, M., & Bhattacharya, T. (2023). Garbage to Gains: The role of biochar in sustainable soil quality improvement, arsenic remediation, and crop yield enhancement. *Chemosphere*, *344*. https://doi.org/10.1016/j.chemosphere.2023.140417

Li, Q. W., Liang, J. F., Zhang, X. Y., Feng, J. G., Song, M. H., & Gao, J. Q. (2021). Biochar addition affects root morphology and nitrogen uptake capacity in common reed (Phragmites australis). *Science of the Total Environment*, *766*. https://doi.org/10.1016/j.scitotenv.2020.144381

Li, W., Wang, J., Chen, X., Mosa, A., Ling, W., & Gao, Y. (2025). Interaction and sorption mechanisms of phthalate plasticizers and Cd2+ on biochar. *Environmental Pollution*, *373*. https://doi.org/10.1016/j.envpol.2025.126176

Liu, P., Sun, S., Huang, S., Wu, Y., Li, X., Wei, X., & Wu, S. (2024). KOH Activation Mechanism in the Preparation of Brewer's Spent Grain-Based Activated Carbons. *Catalysts*, *14*(11). https://doi.org/10.3390/catal14110814

Liu, X., Li, G., Chen, C., Zhang, X., Zhou, K., & Long, X. (2022). Banana Stem and Leaf Biochar as an Effective Adsorbent for Cadmium and Lead in Aqueous Solution. *Scientific Reports* , *12*(1), 1–14. https://doi.org/10.1038/s41598-022-05652-7

Long, Y., Tian, H., Lee, C. H., Li, H., Zeng, Z., Yang, Z., Zhu, G., Chen, X., & Liu, L. (2025). Competitive adsorption of H2O and CO2 on nitrogen-doped biochar with rich-oxygen functional groups. *Separation and Purification Technology*, *359*. https://doi.org/10.1016/j.seppur.2024.130476

M, S. C., & Gupta, S. (2025). Carbon sequestration in cementitious composites containing two-step thermochemically activated biochar. *Cement and Concrete Composites*, *164*. https://doi.org/10.1016/j.cemconcomp.2025.106255

Ma, Y., Xu, Y., Liu, F., Zhang, Y., & Wang, J. (2025). Surface chemical modulation of nitrogen-doped microporous carbon for efficient removal of H2S and CO2: The effect of nitrogen functionality. *Microporous and Mesoporous Materials*, *387*. https://doi.org/10.1016/j.micromeso.2025.113517

Monteagudo, J. M., Durán, A., Alonso, M., & Stoica, A. I. (2025). Investigation of effectiveness of KOH-activated olive pomace biochar for efficient direct air capture of CO2. *Separation and Purification Technology*, *352*. https://doi.org/10.1016/j.seppur.2024.127997

Monteagudo, J. M., Durán, A., Zhao, Y., & Monteagudo, J. (2026). CO2 capture by olive pomace biochar: Effect of relative humidity, isosteric heat of adsorption, and a preliminary Life Cycle Assessment investigation. *Separation and Purification Technology*, *385*, 136445. https://doi.org/10.1016/J.SEPPUR.2025.136445

Nandiyanto, A. B. D., Ragadhita, R., & Fiandini, M. (2023). Interpretation of Fourier Transform Infrared Spectra (FTIR): A Practical Approach in the Polymer/Plastic Thermal Decomposition. *Indonesian Journal of Science and Technology*, *8*(1), 113–126. https://doi.org/10.17509/ijost.v8i1.53297

Naseem, M., Iqbal, S., Malik, H., Awais, M., Jehan, S., & Jabeen, S. (2024). Environmental implications of biochar. In *Biochar - Solid Carbon for Sustainable Agriculture* (pp. 109–125). Bentham Science Publishers. https://doi.org/10.2174/9789815238068124010009

Ong C.K., Ghazali N.F., Hasbullah H., Ismail A.F., Rahman S.A., Kusworo T.D., Lee C.T., 2024, Biomass-Based Biochar as Adsorbent: A Mini Review of Production Methods, Characterization, and Sustainable Applications, *Chemical Engineering Transactions*, 113, 493-498. https://doi.org/10.3303/CET24113083

Peng, Z., Liu, S., Long, Y., Xiao, M., & Feng, H. (2023). Lattice Boltzmann Simulation of the Kinetics Process of Methane Diffusion with the Adsorption-Desorption Hysteresis Effect in Coal. *ACS Omega*, *8*(34), 31135–31144. https://doi.org/10.1021/acsomega.3c03095

Pradhan, C., Ghosh A.K, Singh, P., & Gadhwal, R. (2024). Agroforestry Systems: An Effective Toolfor Carbon Sequestration. In *Sustainable Management and Conservation of Environmental Resources in India* (pp. 181–206). Apple Academic Press. https://doi.org/10.1201/9781003469278-8

Premchand, P., Demichelis, F., Galletti, C., Chiaramonti, D., Bensaid, S., Antunes, E., & Fino, D. (2024). Enhancing biochar production: A technical analysis of the combined influence of chemical activation (KOH and NaOH) and pyrolysis atmospheres (N2/CO2) on yields and properties of rice husk-derived biochar. *Journal of Environmental Management*, *370*. https://doi.org/10.1016/j.jenvman.2024.123034

Promakhova, E. V., Kuksina, L. V., & Galosov, V. N. (2019). Extreme Erosion Events and Climate Change. In *Springer Proceedings in Earth and Environmental Sciences* (pp. 118–120). https://doi.org/10.1007/978-3-030-03646-1_22

Qu, J., Wang, Y., Tian, X., Jiang, Z., Deng, F., Tao, Y., Jiang, Q., Wang, L., & Zhang, Y. (2021). KOH-Activated Porous Biochar with High Specific Surface Area for Adsorptive Removal of Chromium (VI) and Naphthalene from Water: Affecting Factors, Mechanisms and Reusability Exploration. *Journal of Hazardous Materials*, *401*. https://doi.org/10.1016/j.jhazmat.2020.123292

Quan, C., Zhou, Y., Wang, J., Wu, C., & Gao, N. (2023). Biomass-based carbon materials for CO2capture: A review. In *Journal of CO2 Utilization* (Vol. 68). Elsevier Ltd. https://doi.org/10.1016/j.jcou.2022.102373

Rahman, Maryono, & Sigiro, O. N. (2023). What is the True Carbon Fraction Value of Mangrove Biomass. *Malaysian Journal of Science*, *42*(2), 67–72. https://doi.org/10.22452/mjs.vol42no2.10

Ringsby, A. J., Ross, C. M., & Maher, K. (2024). Sorption of Soil Carbon Dioxide by Biochar and Engineered Porous Carbons. *Environmental Science and Technology*, *58*(19), 8313–8325. https://doi.org/10.1021/acs.est.4c02015

Sivaraman, S., Shanmugam, S. R., Venkatachalam, P., Shanmugam, R., Chan Basha, A., & Saady, N. M. C. (2025). Effect of pretreatment type on the physico-chemical properties of activated carbons derived from an invasive weed Prosopis juliflora: potential applications. *Materials Research Express*, *12*(1). https://doi.org/10.1088/2053-1591/ada5c4

Song, H., Wang, J., Garg, A., & Lin, S. (2024). Exploring mechanism of five chemically treated biochars in adsorbing ammonium from wastewater: understanding role of physiochemical characteristics. *Biomass Conversion and Biorefinery*, *14*(5), 5847–5859. https://doi.org/10.1007/s13399-020-01135-9

Standardized Product Definition and Product Testing Guidelines for Biochar That Is Used in Soil (aka IBI Biochar Standards). (n.d.). Retrieved http://www.biochar-international.org/characterizationstandard.

Wang, L., Luo, P., Jiang, C., Shen, J., Liu, F., Xiao, R., & Wu, J. (2023). Distinct effects of biochar addition on soil macropore characteristics at different depths in a double-rice paddy field. *Science of the Total Environment*, *857*. https://doi.org/10.1016/j.scitotenv.2022.159368

Wijitkosum, S. (2022). Biochar derived from agricultural wastes and wood residues for sustainable agricultural and environmental applications. *International Soil and Water Conservation Research*, *10*(2), 335–341. https://doi.org/10.1016/j.iswcr.2021.09.006

Wolicki, R. D., Barbacane, N., Ciulla, M., Arca, S., D'Alessandro, E., Parisi, P., Morodei, F., & Di Profio, P. (2024). Possible Alternative to Established CCS Technologies: Technical and Economical Evaluation. *Society of Petroleum Engineers*. https://doi.org/10.2118/223362-MS

Xiao, X., Chen, B., Chen, Z., Zhu, L., & Schnoor, J. L. (2018). Insight into Multiple and Multilevel Structures of Biochars and Their Potential Environmental Applications: A Critical Review. In *Environmental Science and Technology* (Vol. 52, Number 9, pp. 5027–5047).

American Chemical Society. https://doi.org/10.1021/acs.est.7b06487

Xie, T., He, J., Xu, L.-C., Yan, T., Pan, Q.-W., Wang, L.-W., & Pan, W.-G. (2025). Preparation of N-doped porous biochar with high CO2 adsorption performance via one-step molten salt thermal treatment. *Chemical Engineering Journal*, *521*, 166621. https://doi.org/10.1016/j.cej.2025.166621

Yadav, N. K., Singh, S. K., Patel, A. B., Meitei, M. M., Meena, D. K., Yadav, M. K., Lal, J., & Choudhary, B. K. (2023). Biochar production methods vis-a-vis aquaculture applications: a strategy for sustainable paradigm. In *Organic Farming: Global Perspectives and Methods, Second Edition* (pp. 537–559). Elsevier. https://doi.org/10.1016/B978-0-323-99145-2.00010-0

Yan, L., Gao, G., Lu, M., Riaz, M., Zhang, M., Tong, K., Yu, H., Yang, Y., Hao, W., & Niu, Y. (2024). Insight into the Amelioration Effect of Nitric Acid-Modified Biochar on Saline Soil Physicochemical Properties and Plant Growth. *Plants*, *13*(23). https://doi.org/10.3390/plants13233434

Zhang, C., Ji, Y., Li, C., Zhang, Y., Sun, S., Xu, Y., Jliang L, & Wu, C. (2023). The application of biochar for CO2 capture: influence of biochar preparation and CO2 capture reactors. *Ind. Eng. Chem. Res*, *62*, 17168–17181. doi: 10.1021/acs.iecr.3c00445

Zhang, J., Shao, J., Jin, Q., Zhang, X., Yang, H., Chen, Y., Zhang, S., & Chen, H. (2020). Effect of Deashing on Activation Process and Lead Adsorption Capacities of Sludge-Based Biochar. *Science of The Total Environment*, *716*, 137016. https://doi.org/10.1016/J.SCITOTENV.2020.137016

Zhang, Y., Jin, Y., Li, S., Wu, H., & Luo, H. (2024). Preparation of pistachio shell-based porous carbon and its adsorption performance for low concentration CO2. *Particuology*, *95*, 103–114. https://doi.org/10.1016/j.partic.2024.09.015

Zhi, F., Wang, Y., Wang, J., Zhang, B., Qu, J., Hou, X., Zhao, Y., & Hu, Q. (2025). Advanced biochar for accelerated and efficient pollutant removal in complex water systems. *Separation and Purification Technology*, *363*. https://doi.org/10.1016/j.seppur.2025.132133